Dissipation at tidal and seismic frequencies in a melt-free Moon

F. Nimmo,[1] U. H. Faul,[2] and E. J. Garnero[3]

Received 12 June 2012; revised 10 August 2012; accepted 14 August 2012; published 21 September 2012.

[1] We calculate viscoelastic dissipation in the Moon using a rheological (extended Burgers) model based on laboratory deformation of melt-free polycrystalline olivine. Lunar temperature structures are calculated assuming steady state conduction with variable internal heat production and core heat flux. Successful models can reproduce the dissipation factor (Q) measured at both tidal and seismic frequencies, and the tidal Love numbers h_2 and k_2, without requiring any mantle melting. However, the frequency-dependence of our model Q at tidal periods has the opposite sign to that observed. Using the apparently unrelaxed nature of the core-mantle boundary (CMB), the best fit models require mantle grain sizes of $\sim$1 cm and CMB temperatures of $\approx$1700 K. If melt or volatiles are present, the lunar temperature structure must be colder than our melt-free models. We estimate a present-day mantle heat production rate of 9–10 nWm^{-3}, suggesting that roughly half of the Moon's radiogenic elements are in the crust.

Citation: Nimmo, F., U. H. Faul, and E. J. Garnero (2012), Dissipation at tidal and seismic frequencies in a melt-free Moon, *J. Geophys. Res.*, *117*, E09005, doi:10.1029/2012JE004160.

1. Introduction

[2] Determining the present-day temperature structure of the Moon is both important and challenging [e.g., *Wieczorek et al.*, 2006]. Doing so would provide constraints on its thermal (and perhaps orbital) evolution, and on its inventory of radiogenic elements. The thermal structure of the Moon also controls its mechanical properties: how far down moonquakes occur; the thickness of the near-surface elastic layer; and in particular whether melt is present in the deep mantle [*Weber et al.*, 2011]. The challenge arises from the relative paucity of observations - summarized in section 2.1 below - compared to those available for the Earth.

[3] On being deformed, real geological materials dissipate energy at a rate that depends mainly on temperature and melt and volatile content [*Jackson*, 2007]. Observational measurements of lunar dissipation are available at both seismic ($\sim$ second) and tidal ($\sim$ monthly) periods. The aim of this paper is to use the strong dependence of dissipation on temperature to probe the temperature structure of the Moon. More specifically, it focuses on whether a deep, partially molten mantle layer is *required.* Such a layer would not only place a strong constraint on the lunar temperature structure and evolution; it would also affect the heat flux out of the core (and thus the potential for an ancient lunar dynamo), it would tend to sequester incompatible elements (including radiogenics and volatiles), and it would affect the ability of the lower mantle to relax to an equipotential shape. However, evidence for such a layer based on seismic velocity models, as discussed below, is equivocal [*Garcia et al.*, 2011; *Weber et al.*, 2011]. Dissipation provides a potentially sensitive alternative approach to probing whether such a layer exists.

[4] Our philosophy is to develop a simple model described by a few key parameters, and then to explore a wide range of parameter space. This approach allows us to construct an internally self-consistent, albeit simplified, model. While doing so inevitably neglects details (such as secondary minerals), we argue below that these details are unlikely to matter compared to the uncertainties in the key parameters (such as grain size). In particular, our main focus here is to investigate whether the lunar observations can be reproduced without melt in the mantle. Although volatiles have an important effect on rheology [e.g., *Karato et al.*, 1986; *Hirth and Kohlstedt*, 2003; *Aizawa et al.*, 2008], for this work we assume that the lunar interior is anhydrous. While recent work [e.g., *Hauri et al.*, 2011] has confirmed abundant volatiles in some lunar samples, the bulk volatile inventory is still unclear. We defer examination of the effects of a wet lunar interior to future work. However, we do discuss the likely trade-off between factors not included in our model (e.g., volatiles and melt) and our inferred temperature structure.

[5] We use a forward, rather than an inverse, modeling approach. We can do so because of the limited number of parameters employed, and prefer this approach because it makes the dependence of our results on the parameters easier to assess.

[6] We conclude that a wide range of models are capable of matching the observational constraints, without requiring mantle melting. A similar study of terrestrial dissipation and seismic velocities [*Faul and Jackson*, 2005] also concluded that melting was not required to explain the first-order thermal structure of the upper mantle away from melt-producing

[1]Department of Earth and Planetary Sciences, University of California, Santa Cruz, California, USA.
[2]Department of Earth Sciences, Boston University, Boston, Massachusetts, USA.
[3]School of Earth and Space Exploration, Arizona State University, Tempe, Arizona, USA.

Corresponding author: F. Nimmo, Department of Earth and Planetary Sciences, University of California, Santa Cruz, Santa Cruz, CA 95064, USA. (fnimmo@es.ucsc.edu)

0148-0227/12/2012JE004160

regions such as mid-ocean ridges. The parameter space of successful models considered here is reduced by introducing the additional constraint that the core-mantle boundary remain unrelaxed (see section 4.3).

2. Background

[7] The density and rigidity structure of the Moon have been modeled ever since the acquisition of seismology and gravity data (see *Wieczorek et al.* [2006] and *Lognonne and Johnson* [2007] for recent reviews). However, few attempts have been made to also include quantitative constraints based on dissipation at tidal and seismic frequencies, as we present here. One important exception is the work by *Khan et al.* [2004] and *Khan and Moosegaard* [2005], in which seismic data were combined with geodetic constraints on dissipation and the Love numbers k_2, h_2 to argue for an iron core. However, these works did not interpret the results in terms of a rheological model (which provides a link to temperature, relaxation etc.).

[8] *Williams et al.* [2001] carried out very comprehensive modeling of lunar laser ranging (LLR) data, but did not include the seismic observations or interpret the mantle dissipation data in the context of a rheological model. *Efroimsky* [2012] briefly discusses the case of the Moon in developing a general rheological model. *Lognonne and Mosser* [1993] focus mainly on the seismic dissipation of the Moon, but mention briefly bulk tidal dissipation in the context of Mars. *Nakamura* [2005] pointed out that the absence of detected farside moonquakes could be the result of a deep dissipative layer.

2.1. Observational Constraints

[9] At elevated temperatures, real geological materials are dissipative when subjected to oscillating stresses. One way of quantifying the extent of dissipation is to define a parameter $Q = E_{max}/2\pi\Delta E$, where E_{max} is the peak energy stored during a cycle and ΔE is the energy dissipated per cycle. Thus, Q^{-1} can be thought of as the fraction of energy lost per cycle. For weakly dissipative materials, Q^{-1} approximates the phase lag between forcing and response, though in general this relationship can be quite complex [*Efroimsky and Williams*, 2009].

[10] Values of Q for planets are typically obtained via two different methods. At short periods ($\sim$1–10^3 s) Q can be inferred seismologically by measuring the decay in amplitude of body waves or normal modes [e.g., *Shito et al.*, 2004]. Such methods typically provide some depth-resolution on Q. Seismological studies of lunar Q are difficult for several reasons. There are two mechanisms which reduce the amplitude of observed seismic waves: attenuation due to intrinsic dissipation, and scattering (which redirects the wave energy, and is dominant in the near-surface) [*Blanchette-Guertin et al.*, 2012]. Furthermore, the lowermost mantle of the Moon is very poorly sampled, so Q at depth is poorly constrained [e.g., *Lognonne*, 2005].

[11] At long periods, constraints on the bulk Q of the Moon come from LLR observations, particularly measurement of the angular lag of the Moon's rotation pole from its expected position [*Williams et al.*, 2001]. Determining the solid-body Q requires the effect of fluid dissipation at the core-mantle boundary to be removed, which introduces uncertainty. Furthermore, the *Williams et al.* [2001] approach assumes a frequency-independent k_2, which may not be strictly correct (see Figure 3 below). Bearing these caveats in mind, *Williams et al.* [2001] found $Q = 38.9 \pm 5.4$ at a period of 27.21 days, and a frequency-dependence of $\alpha = -0.17 \pm 0.13$ (see equation (1) below). More recent analysis suggests that $Q \sim 35$ at monthly periods, with a weaker but still negative frequency-dependence [*Williams et al.*, 2012]. The long-period behavior of the Moon thus differs from the usual response of increasing dissipation with increasing period. We discuss this issue further below.

[12] The tidal Love numbers k_2 and h_2 are a measure of how deformable a body is at a particular frequency. Because LLR is more sensitive to the lumped parameter k_2/Q (= $Im(k_2)$) than to Q itself [*Williams et al.*, 2001], uncertainties in k_2 result in uncertainties in Q. Current estimates of k_2 from gravity (0.0255 ± 0.0016 according to *Goossens et al.* [2011]) are comparable to the most recent LLR value of 0.0241 ± 0.0020 [*Williams et al.*, 2012]. The lunar tidal Love number h_2 has been estimated by *Williams et al.* [2001] as $0.034–0.041 \pm 0.018$ and more recently by *Williams et al.* [2012] as 0.048 ± 0.008.

[13] An intriguing result from LLR is that the lunar core-mantle boundary (CMB) appears not to have the expected equilibrium shape [*Williams et al.*, 2012]. The lunar surface does not have the expected equilibrium shape either, probably because it "froze in" its shape at some time in the past [e.g., *Garrick-Bethell et al.*, 2006]. However, for the CMB to be out of equilibrium implies a long relaxation timescale, which is surprising given the likely high temperatures (and suspected presence of melt). In section 4.3 we will examine whether this result is compatible with our models.

[14] Seismological quantification of dissipation in the deep Moon is challenging for several reasons, including band-limited seismic sensors, significant noise levels, and strong wave scattering in the near-surface. Furthermore, waveform interpretation may be complicated by lateral variations in mechanical properties of the lunar interior. Nonetheless, several seismological studies have concluded that the lower lunar mantle is significantly more dissipative than the upper mantle [e.g., *Lognonne and Mosser*, 1993; *Nakamura*, 2005]. More tentatively, there is some evidence that the shear Q in the lunar upper mantle shows a frequency dependence with a slope of roughly 0.7 [*Nakamura and Koyama*, 1982], perhaps due to scattering [*Blanchette-Guertin et al.*, 2012]. Some models also include a reduction in shear wave velocity within the lower mantle [*Weber et al.*, 2011], although others do not [*Garcia et al.*, 2011]. One possible interpretation of this observation is the presence of melt in the deep mantle [cf *Nakamura*, 2005].

[15] As well as quantifying dissipation, seismology provides other important constraints. At least in the upper mantle, determinations of elastic moduli and density have been used to infer both temperature profiles and mineralogy [e.g., *Gagnepain-Beyneix et al.*, 2006; *Khan et al.*, 2007; *Kuskov and Kronrod*, 2009]. While we focus below mainly on Q, we will ensure that our model results are consistent with these inferred moduli and densities. Seismic observations have also been used to argue for a fluid outer core [*Weber et al.*, 2011; *Garcia et al.*, 2011], and also a solid inner core [*Weber et al.*, 2011].

2.2. Laboratory Experiments

[16] Several different groups have carried out torsional oscillation experiments on polycrystalline olivine samples,

with broadly similar results [e.g., *Gribb and Cooper*, 1998; *Jackson et al.*, 2004]. In particular, in the absence of melting, dissipation tends to increase with period; this functional relationship may be written

$$Q^{-1} \sim \omega^{-\alpha}. \quad (1)$$

Here ω is angular frequency (= 2π/period) and α is a constant ≈0.3. This value of α is not what would be expected from the most commonly used model for planetary applications, Maxwell viscoelasticity. In a Maxwell viscoelastic body, $Q^{-1} = G/\eta\omega$ (i.e., $\alpha = 1$), where η is viscosity and G is rigidity [e.g., *Findley et al.*, 1989].

[17] The failure of the Maxwell model to reproduce equation (1) has led to the development of other rheological models. One is the Burgers model, which adds a transient creep component to the rheology [e.g., *Faul and Jackson*, 2005]. In the frequency domain this anelastic behavior is modeled by a distribution of relaxation times, reproducing the observed mild frequency-dependence of Q (equation (1)) [*Jackson and Faul*, 2010]. This "absorption band" mechanism [e.g., *Minster and Anderson*, 1981] is parameterized by the period range over which it operates, and is inferred to arise from the operation of physical processes such as grain boundary sliding [e.g., *Raj and Ashby*, 1971].

3. Model

[18] As noted above, our aim is to develop a simple forward model described by a few key parameters, and then to explore the effects of varying those parameters. We describe the various aspects of such a model below; particular attention is paid to the dissipation model, as that is the effect of most interest.

3.1. Dissipation

[19] For a viscoelastic material, there is phase lag between the applied stress and the strain response which results in dissipation. Treating the elastic moduli as complex quantities (i.e., having phase as well as magnitude) thus provides a convenient description of viscoelastic dissipation. Specifically, the complex shear modulus is written $G^* = 1/J^*$, where J^* is the complex compliance [e.g., *Findley et al.*, 1989]. The complex compliance $J^* = J_r + iJ_i$, where J_r and J_i are the real and imaginary parts, respectively, and $i = \sqrt{-1}$. At a particular frequency the dissipation factor is simply given by $Q^{-1} = J_i/J_r$ and the shear modulus by $G^{-1} = \sqrt{J_r^2 + J_i^2}$.

[20] In general, J^* is frequency-dependent. In the particular case of the extended Burgers model, we have [*Jackson and Faul*, 2010]

$$J_r(\omega) = \frac{1}{G_U}\left[1 + \Delta\int_{\tau_L}^{\tau_H} \frac{D(\tau)d\tau}{(1+\omega^2\tau^2)}\right] \quad (2)$$

and

$$J_i(\omega) = \frac{1}{G_U}\left[\omega\Delta\int_{\tau_L}^{\tau_H} \frac{\tau D(\tau)d\tau}{(1+\omega^2\tau^2)} + \frac{1}{\omega\tau_M}\right] \quad (3)$$

[21] Here $G_U = 1/J_U$ is the unrelaxed (infinite-frequency) shear modulus, τ is a dummy variable with units of time, $\tau_M = \eta/G_U$ is the Maxwell time for viscous relaxation, Δ describes the strength of the relevant relaxation mechanism, ω is the angular frequency, $D(\tau)$ is a distribution of relaxation times and τ_L and τ_H are the integration limits corresponding to short and long periods, respectively. In the low-frequency limit, equation (3) reduces to Maxwellian behavior, in which $J_i = (\omega\eta)^{-1}$.

[22] The high-temperature background distribution of relaxation times D_B, inferred to be due to a diffusive process, is often modeled [e.g., *Minster and Anderson*, 1981] with an absorption-band equation having the following form:

$$D_B(\tau) = \frac{\alpha\tau^{\alpha-1}}{\tau_H^\alpha - \tau_L^\alpha} \quad (4)$$

where $0 < \alpha < 1$ for $\tau_L < \tau < \tau_H$, $\alpha = 0$ elsewhere and here the relaxation strength is given by Δ_B.

[23] The emergence of a plateau (peak) in dissipation, D_P, superimposed on the background, in the experimental data of *Jackson and Faul* [2010] was modeled with a contribution of the form

$$D_P(\tau) = \frac{1}{\tau\sigma\sqrt{2\pi}}\exp\left[\frac{-(\ln(\tau/\tau_P)/\sigma)^2}{2}\right] \quad (5)$$

where the peak position is at $\tau = \tau_P$, peak width is determined by σ and the relaxation strength is described by $\Delta = \Delta_P$. This peak occurs at relatively low temperatures/ short timescales and is inferred to correspond to elastically accommodated grain boundary sliding [*Jackson and Faul*, 2010; *Morris and Jackson*, 2009].

[24] Because of the strong dependence of timescale on viscosity and thus temperature, the four timescales τ_L, τ_H, τ_P and τ_M are all normalized to respective values τ_{iR} (where $i = L, H, P, M$) at a particular reference pressure P_R, temperature T_R and grain size d_R:

$$\tau_i(P,T,d) = \tau_{iR}\left(\frac{d}{d_R}\right)^m \exp\left[\left(\frac{E}{R}\right)\left(\frac{1}{T} - \frac{1}{T_R}\right)\right]\exp\left[\left(\frac{V}{R}\right)\left(\frac{P}{T} - \frac{P_R}{T_R}\right)\right] \quad (6)$$

[25] Note that there are potentially two grain-size exponents: one for anelastic processes (m_a for $i = L, H, P$) and one for long-term viscous creep (m_v for $i = M$). The approach employed here automatically accounts for the frequency-, grain-size and temperature-dependence of the system response [*Jackson et al.*, 2004] and is similar in effect to the temperature-dependent frequency cutoff adopted by *Lognonne and Mosser* [1993] in their discussion of lunar seismology.

[26] We also calculate the pressure- and temperature-sensitivity of the unrelaxed modulus:

$$J_U(T,P) = \left[G_U(T_R,P_R) + (T-T_R)\frac{\partial G}{\partial T} + (P-P_R)\frac{\partial G}{\partial P}\right]^{-1} \quad (7)$$

where $\frac{\partial G}{\partial T}$ and $\frac{\partial G}{\partial P}$ are experimentally measured quantities [*Isaak*, 1992; *Bass*, 1995].

[27] The model described above includes both an absorption band (equation (4)) and a broad absorption peak (equation (5)). This peak is most evident when levels of dissipation are low (large Q), near the experimental resolution

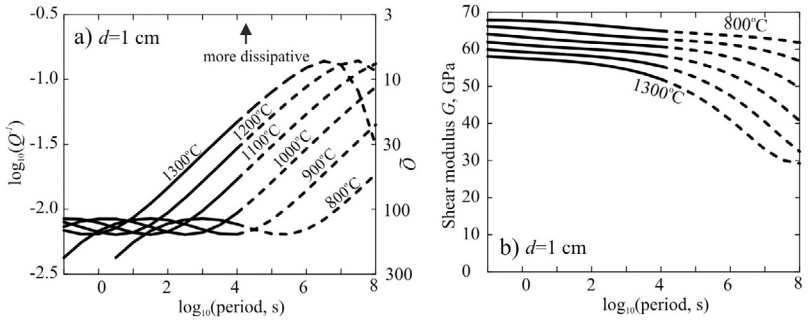

Figure 1. (a) Dissipation (Q^{-1}) as a function of period and temperature calculated using the extended Burgers model (section 3.1) and the parameters given in Table 1 for a grain size of 1 cm. Model predictions at longer periods for which there are no experimental data are indicated by dashed lines; see text. Tidal dissipation within the Moon occurs at these long periods. (b) Shear modulus, calculated as for Figure 1a. Note that shear modulus is less sensitive to temperature variations than is Q.

limit, and is therefore not well resolved. Justification for inclusion of this peak in the fit is derived from a combination of experimental observations and physical arguments. Comparison of the experimental modulus data with the moduli predicted for purely elastic (anharmonic) behavior indicates that some modulus relaxation is taking place just outside the currently experimentally accessible frequency-temperature space. This relaxation can be accounted for by the broad peak. The physical argument for the existence of such a peak is based on a model by *Raj and Ashby* [1971], which has been further developed by *Morris and Jackson* [2009] and *Lee et al.* [2011]. This model describes anelastic relaxation as being due to two grains sliding past each other in response to an applied shear stress. This process consists of two parts: sliding moderated by the viscosity of the grain boundary and opposed by elastic distortions at grain corners, giving rise to an absorption peak; and diffusive processes in response to stress concentrations, giving rise to the absorption band.

[28] Figure 1 uses the model described above to predict the behavior of melt-free polycrystalline olivine over a wide frequency range. The lines are dashed where we have extrapolated beyond the experimentally constrained domain. Figure 1a shows that the broad peak results in near frequency-independent dissipation at short (seismic) periods and relatively low temperatures, while at higher temperatures and longer periods the absorption band gives rise to increasing levels of dissipation with increasing period (α = 0.27; equation (1) and Table 1). Figure 1a also shows that at sufficiently long periods and elevated temperatures, the edge of the absorption band is reached such that dissipation decreases again, before the onset of viscous behavior at even longer periods (α = 1, not shown). However, as noted above the long-period end of the absorption band model, equation (4) - which controls the location of the maximum - is not well constrained.

[29] Figure 1b shows that shear modulus and hence seismic velocity are only mildly affected by the absorption peak, compared with its effect on Q. Generally, the moduli are less temperature-dependent than the dissipation factor, suggesting that dissipation should provide an important role in resolving the thermal structure of the Moon. In addition, dissipation is likely less dependent on composition than are seismic velocities [*Karato*, 2006].

3.2. Temperature Structure

[30] In calculating dissipation a physically realistic model of the Moon's temperature structure is obviously desirable. At the same time, to permit sensitivity analysis the number of free parameters needs to be kept relatively small. *Gagnepain-Beyneix et al.* [2006] faced a similar problem, and employed a somewhat similar approach to the one we adopt here.

[31] We assume a spherically symmetric, three-layer conductive Moon in steady state. The crust (outer radius R) and mantle (outer radius R_d) experience internal heating at rates H_1 and H_2, respectively, while the heat flux at the top of the core (radius R_c) is fixed at F_c. With the surface temperature

Table 1. Model Parameters[a]

Var.	Quantity	Eqn.
d_R	3.1 μm	6
T_R	1173 K	6
P_R	0.2 GPa	6
V	10^{-5} m^{3}mol^{-1}	6
G_U	66.5 GPa	7
$\partial G/\partial T$	−13.6 MPa K^{-1}	7
$\partial G/\partial P$	1.8	7
m_a	1.31	6
Δ_B	1.04	2
α	0.274	4
τ_{LR}	10^{-3} s	6
τ_{HR}	10^{7} s	6
τ_{MR}	$10^{7.48}$ s	6
E	360 kJ/mol	6
Δ_P	0.057	5
τ_{PR}	$10^{-3.4}$ s	6
σ	4	5
m_v	3	6
R	1740 km	9
R_c	400 km	10
g_0	1.62 m s−^{2}	9
ρ_0	3300 kg m^{-3}	9
T_s	250 K	10
k	3 W m^{-1} K^{-1}	10

[a]"Eqn." refers to the equation in which the variable ("Var.") is introduced. Upper part of table details rheological parameters for melt-free polycrystalline Fo_{90} olivine, from Table 2 of *Jackson and Faul* [2010]. Lower part of table gives other parameter values adopted.

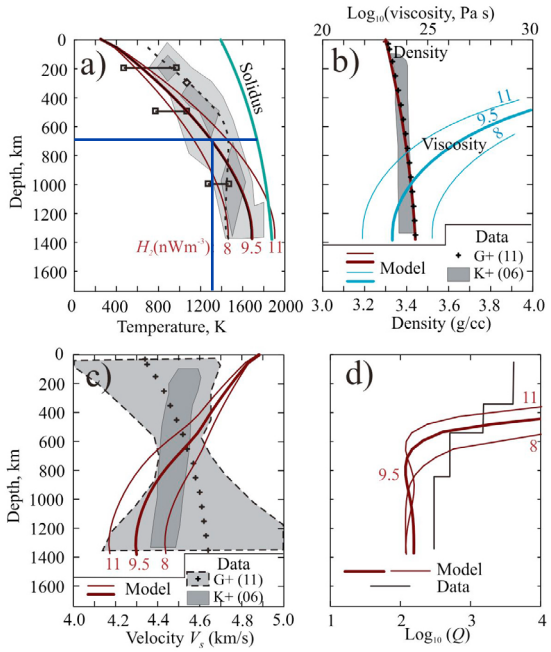

Figure 2. (a) Model lunar crust and mantle temperature structures using equation (8). Here fixed values are R_d = 1695 km (crustal thickness 45 km); R_c = 400 km; H_1 = 160 nWm^{-3} and F_c = 0. The effect of varying the mantle heating rate H_2 is shown; baseline model is in bold. The shaded regions show the probability distribution of the lunar temperature, from joint inversion of multiple data sets, replotted from *Khan et al.* [2006]. Squares joined by lines are from electromagnetic sounding [*Hood et al.*, 1982]; diamond is from retention of mascon topography [*Lambeck and Pullan*, 1980]. Dashed line is a convective model result from *Ziethe et al.* [2009]. Green line is the peridotite solidus of *Hirschmann* [2000]. (b) Model mantle density (equation (9)) and viscosity structure. Density is compared with seismically-inferred values of *Garcia et al.* [2011] and *Khan et al.* [2006]. (c) Model S-wave velocity structure, evaluated at 1s, compared with *Garcia et al.* [2011] and *Khan et al.* [2006] values. (d) Model seismic Q at 1 s calculated using the approach outlined in section 3.1, assuming a grain-size of 1 cm and the baseline temperature profile shown in Figure 2a. For comparison the seismically-inferred Q summarized in *Garcia et al.* [2011] is shown.

fixed at T_s, the temperature $T(r)$ at $R_c \le r \le R_d$ may be shown to be

$$T(r) = T_s - \frac{H_2 r^2}{6k} + \left[\frac{F_c R_c^2}{k} - \frac{H_2 R_c^3}{3k}\right]\left[\frac{1}{r} - \frac{1}{R}\right] + \frac{H_1 R^2}{6k} + \frac{R_d^3(H_1 - H_2)}{3kR} - \frac{R_d^2(H_1 - H_2)}{2k} \quad (8)$$

where k is the thermal conductivity (assumed constant). Taking the crustal thickness ($R - R_d$) and heat production rate H_1 to be known (see below), there remain only two free parameters: the mantle heating rate H_2 and the heat flux out of the core F_c. Given these two values, the temperature at the base of the mantle T_b may be derived. In some situations below we report T_b rather than H_2, since the former provides a more direct link to mantle viscosity and dissipation. For the relatively low core heat fluxes expected at the Moon, the effect of F_c on T_b is small. The deep temperature structure is also not very sensitive to how much radioactive heating takes place in the crust.

3.3. Density

[32] As with temperature, to facilitate sensitivity analysis we adopt a simple approach to describe the density structure. Assuming that gravity varies linearly with radius (a reasonable approximation for the Moon), the density may be written

$$\rho(r) = \rho_0 \left(1 - \frac{\rho_0 g_0 R\left[1 - \frac{r^2}{R^2}\right]}{2K_0}\right)^{-1} \quad (9)$$

where ρ_0 and g_0 are the surface density and acceleration due to gravity, respectively, and K_0 is the bulk modulus (assumed constant, and calculated from the unrelaxed shear modulus assuming a Poisson's ratio of 0.25). Figure 2 shows that this simple approach can still yield a good fit to the seismically inferred density structure. The pressure is calculated analytically taking ρ to be constant; the errors thus introduced do not affect the results significantly.

3.4. Tidal Model

[33] Once the Burgers approach has been used to calculate $G^*(r)$, this quantity is then imported directly into our existing multilayer viscoelastic tidal code [*Roberts and Nimmo*, 2008]. The lunar mantle is discretized into 24 layers of equal thickness, and a viscosity cutoff of 10^{29} Pa s is imposed for numerical reasons. We note that our code assumes incompressibility (i.e., all dissipation is shear-related) and spherical symmetry; to take lateral variations into account would require a different approach [e.g., *Behounkova et al.*, 2010; *Zhong et al.*, 2012]. We also note that our initial attempts to use a multilayered Maxwell rheology were unable to reproduce the apparently weak observed frequency-dependence of long-period lunar Q (section 2.1) - one reason for adopting the extended Burgers model.

3.5. Parameters Adopted

[34] The bulk composition of the lunar mantle is inferred to be similar to that of the Earth, although possibly with a lower Mg# in the upper mantle [e.g., *Wieczorek et al.*, 2006]. In the absence of melt, viscoelastic properties of the Earth's upper mantle are adequately represented by the properties of polycrystalline olivine [*Hirth and Kohlstedt*, 2003; *Faul and Jackson*, 2005]. We therefore adopt the same approach for the Moon, with the relevant model parameters given in Table 1. We neglect the effects of melt because we are interested in whether a melt-free mantle can reproduce the observations. We discuss the effect of likely complications, such as the presence of melt, in section 5.1.

[35] The grain size of the lunar mantle is poorly known. Smaller grain sizes typically result in more rapid creep and enhanced dissipation. In our baseline model we assume a grain size of 1 cm, and explore the effects of varying this parameter in section 4.2. We discuss the likely physical effects controlling lunar mantle grain size in section 5.2.

[36] In contrast to many studies, we pay relatively little attention to the crust. This is because it is volumetrically

small, cold and not dissipative; our main interest is in the deep mantle, where dissipation is significant and melting is most likely. We do however, include the crust in our thermal modeling. We assume that the mantle is compositionally homogeneous, for simplicity. This is consistent with models from several recent studies that lack discontinuities in the mantle [*Khan et al.*, 2007; *Garcia et al.*, 2011].

[37] For the thermal model, we take a crustal thickness of 45 km [*Garrick-Bethell et al.*, 2010], a thermal conductivity of 3 W m^{-1} K^{-1} and a surface temperature T_s of 250 K. Despite the existence of samples, remote sensing data and the Apollo heat flow probes, the radiogenic element budget of the Moon is still uncertain (see SOM section 10 of *Garrick-Bethell et al.* [2010]). Here we take the crustal heating rate to be H_1 = 160 nWm^{-3}, derived from the measured surface abundance of Th [*Jolliff et al.*, 2000]. As will be seen below, our results are not very sensitive to this parameter.

[38] Although there is some uncertainty in the radius of the lunar core R_c, recent seismological work has suggested it is in the range 310–420 km [*Garcia et al.*, 2011; *Weber et al.*, 2011]. In our baseline model we adopt R_c = 400 km, and take a core density of 5000 kg m^{-3} [*Garcia et al.*, 2011]. We adopt a mantle reference density of ρ_0 = 3300 kg m^{-3} to yield results consistent with the densities which *Garcia et al.* [2011] derived by assuming Birch's law. Other models [e.g., *Khan et al.*, 2007; *Kuskov and Kronrod*, 2009] yield slightly different density profiles (Figure 2b), but would not significantly change the calculated values of dissipation or Love numbers. In our baseline model we assume an entirely liquid core (zero rigidity).

4. Results

4.1. Example Lunar Structures

[39] In this section we illustrate the results of applying our method to different lunar temperature structures. Figure 2a plots the crust and mantle temperature structure from equation (8) for three cases in which F_c = 0 and H_2 is varied. Our baseline case (bold line) has H_2 = 9.5 nWm^{-3} and T_b = 1683 K. We also show (green line) a dry peridotite solidus (from *Hirschmann* [2000]), demonstrating that our baseline model is consistent with an absence of present-day melting. A higher value of H_2 would predict melting toward the base of the mantle, but results in a poorer fit to the observational constraints (see section 4.2).

[40] These profiles are superimposed on a modeled probability distribution of lunar temperatures, derived by inverting multiple data sets (primarily seismic travel times) simultaneously [*Khan et al.*, 2006]. Other constraints on mantle temperature are from electromagnetic sounding (squares; *Hood et al.* [1982]) and the ability to sustain mascon topography (diamond; *Lambeck and Pullan* [1980]).

[41] In addition we plot (dashed line) a representative present-day temperature structure from a lunar convection model [*Ziethe et al.*, 2009]. This model assumes a 650 K temperature at the base of the crust to mimic the effects of regolith insulation and crustal heat production. At depth the temperature gradient is shallower, and the bottom temperature is lower (thus preventing melting), than in our models, because of convection. Given the uncertainties in the observational constraints, both convective and conductive models appear viable.

[42] Figure 2b compares the resulting model mantle density profile (equation (9)) with seismically inferred profiles from [*Khan et al.*, 2006] and [*Garcia et al.*, 2011], demonstrating reasonable agreement with both. The baseline viscosity at the base of the mantle is 2×10^{23} Pa s and increases steeply with decreasing depth. This behavior has implications for relaxation to equilibrium shape (see section 4.3 below).

[43] Figure 2c shows our model shear wave velocity ($V_s = \sqrt{G/\rho}$), compared with seismologically determined values obtained by *Khan et al.* [2006] and *Garcia et al.* [2011]. A key model result is that, due to the increasing temperature, model velocities decrease with depth throughout the mantle as lunar pressures are too small to have a significant effect. Velocities calculated for conductively cooling terrestrial oceanic lithosphere show a similar decrease, consistent with seismological observations [*Gaherty and Jordan*, 1995; *Faul and Jackson*, 2005]. Our model profile shows the same trend as the *Khan et al.* [2006] profile, but a greater variation in V_s with depth. At depths greater than about 400 km our baseline model fits within the envelope of V_s values determined by *Garcia et al.* [2011]. However, their best-fit velocity profile shows the opposite depth-dependence to our model results and the *Khan et al.* [2006] profile. The results of *Weber et al.* [2011] are similar to those of *Garcia et al.* [2011], but the former include a low-rigidity layer at the base of the mantle which they ascribe to melting (see below).

[44] The mismatch at shallow depths between our model and the seismically inferred velocities suggest that the upper portion of the lunar mantle may not consist of an olivine-dominated, peridotitic composition [e.g., *Wieczorek et al.*, 2006]. This mismatch, however, is of minor importance to our dissipation and Love number results, since these are influenced mainly by the deep structure.

[45] Figure 2d shows the results of our dissipation calculations (section 3.1) for a grain size of 1 cm. The red lines are the model Q (log scale) at a period of 1 s. The high Q values calculated for the upper ~700 km reflect the fact that at low temperatures the behavior is essentially elastic. The smaller seismically inferred Q values (summarized in *Garcia et al.* [2011]), along with the strong frequency dependence ($\alpha \approx 0.7$) both are consistent with scattering being the dominant process in this depth range. At depths >600 km, our model $Q \approx 100$ is enough to cause significant attenuation of waves from farside earthquakes [*Nakamura*, 2005], without requiring partial melting. The seismically inferred Q in the lower mantle is a factor of ≈2 larger than our model values, although the resolution at this depth is limited.

[46] These results at tidal and seismic frequencies are summarized and compared with the observational constraints in Table 2.

[47] As summarized in Table 2, our baseline model has k_2 = 0.0251, h_2 = 0.0422 and Q = 32 at 2.5×10^6 s; all three are predicted to be weakly frequency-dependent (see below). Our model value agrees with current constraints on k_2 derived from gravity and LLR (see Table 2). Our model also matches the monthly Q value, but the frequency-dependence (α in equation (1)) has the opposite sign to the measured value. The model frequency-dependence is due in part to the parameters τ_H and τ_L (equation (6)), which are not well-constrained by experiments (see sections 3.1 and 5.1).

Table 2. Comparison of Baseline Model Results With Observational Constraints[a]

	k_2	h_2	Q_{tidal}	$Q_{400–800}$	$Q_{800–1200}$	α
Williams et al. [2012] (LLR)	0.0241 ± 0.0020	0.048 ± 0.008	~35	-	-	−0.17 ± 0.13
Goossens et al. [2011] (grav.)	0.0255 ± 0.0016	-	-	-	-	-
Garcia et al. [2011] (seism.)	-	-	-	500	300	-
Baseline model	0.0251	0.0422	32	419	121	+0.16
Model d = 1 mm	0.0274	0.0460	20	243	138	−0.02
Model R_c = 300 km	0.0237	0.0397	37	590	124	+0.17
Model H_1 = 80 nWm^{-3}	0.0251	0.0421	32	439	121	+0.14

[a]Baseline model (Figure 2 and Table 1) has H_2 = 9.5 nWm^{-3}, T_b = 1683 K and d = 1 cm. $Q_{400–800}$ and $Q_{800–1200}$ are volume-averaged Q values over depth ranges of 400–800 and 800–1200 km (evaluated at 0.1 s period in the model). Q_{tidal} is the bulk value, evaluated at 2.5 × 10^6 s in the model. The quantity α is the frequency-dependence of tidal Q (equation (1)); the LLR α value is from *Williams et al.* [2001]. For the d = 1 mm model we keep the temperature structure the same. For the R_c = 300 km and H_1 = 80 nWm^{-3} models, we keep T_b the same, by setting H_2 = 8.94 nWm^{-3} and H_2 = 9.7 nWm^{-3}, respectively. All models have F_c = 0.

[48] The final three rows of Table 2 show the effect of varying some key parameters. Decreasing the grain size (d = 1 mm) while keeping everything else the same results in a more dissipative and deformable Moon, because of the reduction in silicate viscosity. Reducing the core size (R_c = 300 km) while keeping T_b the same has the opposite effect, because (weak) core material has been replaced with (more rigid) silicates. We defer discussion of the role of an inner core to section 5.1. Finally, keeping T_b the same but putting less radiogenic material in the crust has a very small effect on our results, as expected. We investigate the sensitivity of our results to parameter choices more extensively in section 4.2 below.

[49] In summary, Figure 2 shows that the simple temperature structure adopted provides a reasonable match to the observational constraints at both seismic and tidal periods. Importantly, in contrast to the results of *Weber et al.* [2011], no melting is required - a similar conclusion to that of *Faul and Jackson* [2005] for the Earth. In fact, at seismic frequencies our model is slightly too dissipative even without melt - the addition of melt would only exacerbate this problem.

[50] Figure 3 shows how our model Q and Love numbers h_2 and k_2 vary with period. The observed lunar Q and k_2 data are discussed in section 2.1. As noted above, our model Q matches the observations at monthly frequencies, but the frequency-dependence has the wrong sign. We predict that k_2 will be slightly frequency-dependent, a potentially measurable effect.

[51] At seismic frequencies, we plot the model volume-averaged Q in the depth ranges 400–800 km and 800–1200 km. This dissipation is a factor of ≈2 too large (but probably still within the likely measurement uncertainty). The frequency-dependent behavior in the upper mantle is weaker than that inferred by *Nakamura and Koyama* [1982], likely because scattering is not included in our model.

4.2. Parameter Space Exploration

[52] Figures 2 and 3 demonstrate that a reasonable match to the observations can be obtained for melt-free olivine. The next requirement is then to determine what range of parameter space is occupied by successful models. That is the aim of this section.

[53] To quantify the success of a particular model in fitting the observations, we define the misfit χ^2 as follows:

$$\chi^2 = \Sigma_{i=1}^{4} \left(\frac{o_i - m_i}{\sigma_i} \right)^2 \quad (10)$$

where o_i, m_i and σ_i are the observed value, model value and quoted uncertainty, respectively, in the observation. In practice, this value is divided by the minimum value to give a normalized misfit. Here the four observations (Q_{tidal}, h_2, k_2, $Q_{800–1200}$) we use are given in Table 2. For k_2 we take the mean of the two quoted values and use the larger uncertainty estimate. The uncertainties in Q_{tidal} and $Q_{800–1200}$ are not given but are taken to be 5 (14%) and 150 (50%), respectively. We did not use the shallower seismic constraint $Q_{400–800}$ because of the likelihood that it is affected by scattering (which we do not model).

[54] Figures 4a and 4b plot how the normalized misfit varies with T_b and F_c for two different grain sizes. The star denotes the parameter choice shown in Figure 2. There is evidently a tradeoff between these two parameters, yielding pairs of parameters having equally good misfits. The reason is that dissipation depends both on T_b and the thickness of the dissipative layer, which is controlled by F_c. The same bulk dissipation can be achieved with either a high T_b and a relatively thin layer (high F_c), or with lower T_b and a thicker layer. Because viscosity decreases with decreasing grain size, lower values of T_b provide acceptable misfits in the 1 mm case compared with the 1 cm case.

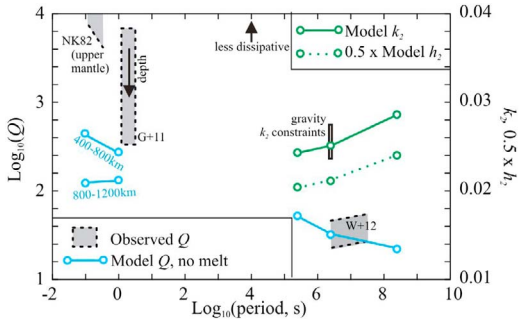

Figure 3. Lunar model and observed Q, h_2 and k_2 as a function of frequency. At seismic frequencies, dissipation is observed to increase with depth; for the upper mantle Q shows a frequency-dependence with a slope α of ≈0.7. Envelope of long-period values is from *Williams et al.* [2012] (see section 2.1) where $Q \sim 35$ at monthly periods and the uncertainties were approximated from earlier constraints on Q by *Williams et al.* [2001]. References: G + 11 [*Garcia et al.*, 2011]; NK82 [*Nakamura and Koyama*, 1982]; W + 12 [*Williams et al.*, 2012].

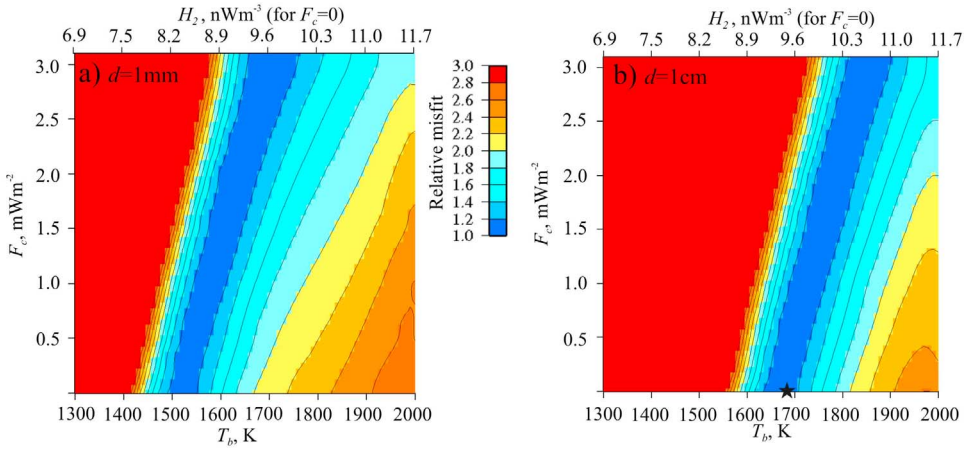

Figure 4. (a) Contours of normalized misfit (equation (10)) as a function of F_c and T_b for a grain size of 1 mm. Note the narrow best-fit region, and the tradeoff between F_c and T_b. We also tabulate H_2 for the case when the core heat flux is zero. (b) As for Figure 4a, but with a grain size of 1 cm. The best-fit region is shifted to higher temperatures. The star denotes our baseline model (Figure 2).

[55] In addition to T_b, Figure 4 also plots the equivalent value of H_2, assuming no core heat flux. For low core heat fluxes, the relatively narrow best-fitting region implies H_2 is in the range 9–10 nWm^{-3}. We discuss the implications of this result further below.

4.3. Relaxation at the CMB

[56] Figure 4 demonstrates that there are a many $T_b - F_c$ pairs which yield equally good fits. How might this degeneracy be reduced?

[57] One possibility is to make use of the tentative geodetic observation that the core-mantle boundary (CMB) of the Moon does not conform to the expected equipotential shape [*Williams et al.*, 2012]. If the lunar core is indeed partly liquid [*Weber et al.*, 2011], this result in turn suggests that the lunar mantle has not yet fully relaxed.

[58] Mantle relaxation is in reality a viscoelastic problem [e.g., *Zhong and Zuber*, 2000]. However, at the high temperatures expected at the base of the mantle, the problem is primarily one of viscous flow in a channel which is thin compared to the (degree-2) wavelength of flow. Furthermore, the ~0.1 MPa stresses associated with the likely CMB deflection [*Williams et al.*, 2012] are small enough that the dominant viscous deformation mechanism - as with the tidal response - is diffusion creep. For this simplified problem, an approximate expression for the relaxation timescale τ of degree-2 topography is given by [*Nimmo and Stevenson*, 2001]

$$\tau \sim \frac{\eta_b R_c^2}{\Delta\rho g_c \delta^3} \sim \frac{\eta_b R_c}{\rho_c \Delta\rho G \delta^3} \tag{11}$$

[59] Here η_b is the viscosity at the base of the mantle, $\Delta\rho$ is the core-mantle density contrast, g_c is the gravity at the CMB, G is the gravitational constant and δ is the effective channel thickness.

[60] The channel thickness δ is given by the distance over which the viscosity increases by a factor e, and depends on the temperature structure near the CMB and the activation energy. The corresponding temperature drop ΔT is given by $\Delta T = R_g T_b^2 / E$ where R_g is the gas constant and E is the activation energy.

[61] Near the CMB, the temperature is changing both because of the heat flux F_c at the CMB and also because of internal heating in the mantle. By linearizing equation (8) around T_b, we can derive the following expression for the channel thickness δ:

$$\delta = \frac{k R_g T_b^2}{E} \left(\frac{2}{3} H_2 R_c + F_c \right)^{-1} \tag{12}$$

[62] This expression displays the right behavior: in the absence of internal heating it reduces to the more usual form [e.g., *Nimmo and Stevenson*, 2001], while the presence of internal heating decreases the temperature gradient near the CMB and thus increases δ.

[63] Figure 5 shows the relaxation times obtained by combining equations (11) and (12) , for the same parameter choices as in Figure 4. High basal temperatures or high heat fluxes result in rapid relaxation. In a similar manner to Figure 4, there is a tradeoff: relaxation happens equally rapidly in a thin channel (high F_c) with a high T_b (low viscosity), or a thicker channel with a lower T_b. However, in the 1 mm case, the minimum misfit region from Figure 4 implies a relaxation time of order 100 Myr, too short to permit an unrelaxed CMB. On the other hand, the 1 cm case has a narrow region in which both the relaxation constraints and the geodetic constraints are satisfied.

5. Discussion

[64] Melt-free olivine is dissipative at high temperatures (Figure 1): dissipative enough to explain terrestrial observations without requiring melting [*Faul and Jackson*, 2005]. In a similar fashion, we showed above that plausible thermal structures of the Moon can yield the observed lunar dissipation without requiring a lower mantle melt layer. We find that relatively large grain sizes (≈1 cm) and high CMB temperatures (≈1700 K) are required to simultaneously satisfy the requirements of dissipation (Figure 4) and absence of CMB relaxation (Figure 5).

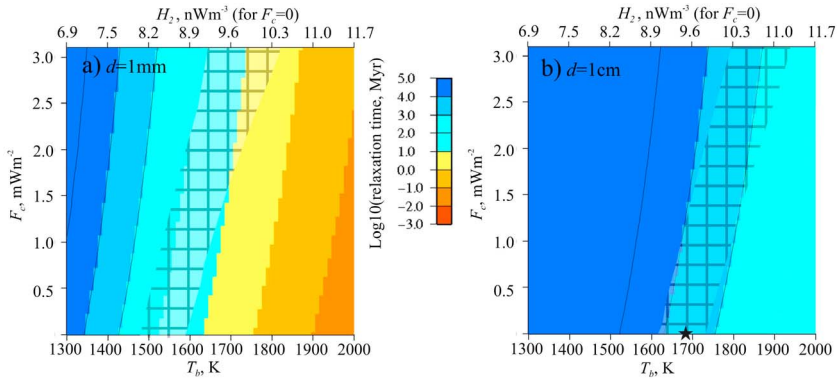

Figure 5. (a) Contours of relaxation time (equation (11)) as a function of F_c and T_b for a grain size of 1 mm. The cross-hatched area denotes best-fitting region from Figure 4a. In this region implied relaxation times are short (∼10 Myr). (b) As for Figure 5a, but for a grain size of 1 cm. Here the best-fit region from Figure 4b is consistent with longer relaxation times (>1 Gyr).

[65] These results are preliminary, because they are based on a highly simplified thermal and petrological model. Below we outline some obvious complications, and how they are likely to affect our conclusions. We also discuss some of the implications of these initial results.

5.1. Complications and Uncertainties

[66] For reasons explained in the Introduction, we adopted a very simplified, melt-free, mono-mineralic mantle. Our baseline model can match the observations, and is consistent with the absence of melt, but is not necessarily realistic.

[67] Long-period dissipation is dominated by the absorption band behavior (equation (4)). The parameter τ_{HR}, which quantifies the long-period limit of this behavior, lies largely outside experimentally accessible periods and is thus poorly constrained. Increasing τ_{HR} to 10^8 s in our baseline model yields h_2, k_2 and Q_{tidal} values of 0.0408, 0.0243 and 53, respectively. This reduction in dissipation can be offset by an increase in H_2 by 7%, yielding T_b = 1785 K. Similarly, decreasing τ_{HR} to 10^6 s gives values of 0.0446, 0.0266 and 22, with a tidal Q that is frequency-independent. The increase in dissipation can be offset by reducing T_b to 1567 K, in which case the Q exhibits a similar frequency-dependence to the baseline case (α = +0.14). Overall, uncertainty in τ_{HR} yields an uncertainty of ±100 K in the basal temperature estimate.

[68] We have endeavored to match the observed Q_{tidal}, but in none of the cases we examined could we simultaneously match the observed frequency-dependence of this quantity (Figure 3). This discrepancy deserves comment. The observation is hard to make, and the reported strength of the frequency-dependence has changed over time [*Williams et al.*, 2001, 2012]. Nonetheless, it may be a real effect, and our best-fit models do not reproduce it. A grain size of 1 mm with T_b = 1683 K does have a tidal Q which is frequency-independent, but provides a poor fit otherwise (Table 2). One possibility is that the extrapolation to longer periods (section 4.1) is the problem. Alternatively, the effects of water and/or melt, which we have not taken into account, can significantly alter the dissipative behavior. In particular, melt can reduce and potentially even change the sign of α [*Jackson et al.*, 2004]. Future work should address this issue.

[69] The ≈1700 K basal temperatures obtained in this study are consistent with an absence of mantle (peridotite) melting (Figure 2a). At the same time, they are also consistent with the presence of a fluid iron core, especially if it is sulphur-rich [*Weber et al.*, 2011]. How the apparently volatile-depleted Moon could have retained sulphur in its core presents a puzzle for the future.

[70] Very few experimental observations exist on the effect of composition on attenuation, but the effects are probably modest [*Karato*, 2006]. Any factors increasing attenuation, such as water [*Karato and Jung*, 1998], melt [*Jackson et al.*, 2004; *Faul et al.*, 2004] or dislocations [*Farla et al.*, 2012], would require a reduction in temperature in order to match the dissipation constraints. Similarly, the presence of water lowers the effective viscosity [*Hirth and Kohlstedt*, 2003] and would make CMB relaxation more likely. Thus, our melt-free model temperature results effectively represent an upper bound.

[71] Another potential source of dissipation is the solid inner core, if it exists. The magnitude of the dissipation will depend on the poorly known viscosity of this material. We also note that torques and dissipation at the surface of the inner core may affect the LLR constraints on the fluid core moment.

[72] Our baseline model has zero core heat flux. This is partly because of model results suggesting that F_c should be low [e.g., *Ziethe et al.*, 2009], but also because doing so results in a more self-consistent picture (T_b should not be so high that melting of secondary phases occurs). If the core heat flux were higher, the inferred mantle temperatures would be also be higher (Figure 4).

[73] Our steady state conductive temperature structure differs appreciably from models in which convection operates (Figure 2a), but whether the lunar mantle is convecting at the present-day is unclear. Our baseline model yields a basal Rayleigh number of ∼10^3, insufficient to initiate convection in strongly temperature-dependent silicates. Thus, our assumption of conduction is at least internally self-consistent. A perhaps more serious problem is that our assumption of uniform heating within the mantle is too simple. Vertical variations in mantle heat production are a likely consequence of progressive magma ocean crystallization [*Wieczorek et al.*, 2006]. *Gagnepain-Beyneix et al.* [2006] assumed variable heat production in a conductive mantle and found temperatures of 1175–1250°C at 1000 km depth, a little colder than our

nominal value of 1282°C. Detailed investigation of the effect of such variations should certainly be attempted in future.

[74] Finally, our model has assumed a spherically symmetric Moon. The real Moon demonstrates regional lateral heterogeneity [e.g., *Jolliff et al.*, 2000], though whether this heterogeneity extends to depth is not yet clear. At any event, given the uncertainties in other parameters of interest, it is currently hard to justify the complexities which a 3D model would require.

5.2. Implications

[75] The inferred lunar mantle grain size of ~1 cm is within the range of grain sizes inferred for the terrestrial upper mantle. In the Earth's mantle, and likely the early Moon, when convective stresses were high enough to cause dislocation creep, grain size will have been controlled by two competing processes: grain growth due to surface energy reduction; and grain size reduction due to recrystallization driven by mantle deformation [*Karato*, 1988]. At present grain growth may be effectively inhibited by secondary phases as well as relatively low temperatures, while stress and strain in the Moon are probably too small to cause recrystallization.

[76] Because dissipation is most affected by deep temperature structure, our results are not very sensitive to crustal heat production. The final model in Table 2 has a crustal heat production rate half that of the baseline model, and yet the results are almost identical. The corresponding total heat production rates are 0.33 TW (8.7 mW m^{-2}) and 0.46 TW (12 mW m^{-2}). The higher (baseline) surface heat flux is consistent with a revised Apollo 17 heat flux estimate [*Rasmussen and Warren*, 1985].

[77] The uncertain effect of the crust means that total heat production is not well-constrained. However, Figure 4 suggests that for low core heat fluxes, mantle heat production rates are in the range 9–10 nWm^{-3}. *Gagnepain-Beyneix et al.* [2006] obtained mantle concentrations of 8.2 ppb U and 30 ppb Th; assuming a K/U ratio of 2000, the resulting heat production rate is about 6 nWm^{-3}, somewhat lower than our values. By comparing these results with the admittedly uncertain bulk lunar heat production rate of 22 nWm^{-3} inferred by *Garrick-Bethell et al.* [2010], it appears that roughly half of all heat-producing elements are contained within the lunar crust. Removal of radiogenic elements from depth to the crust results in increased cooling rates, and illustrates the importance of volcanism (and attendant transport of incompatibles) in planetary thermal evolution [cf. *Ziethe et al.*, 2009].

5.3. Future Work

[78] Given the importance of determining the bulk lunar volatile abundance [e.g., *Hauri et al.*, 2011], it would be desirable to extend the work presented here to water-bearing systems. As summarized in *Jackson* [2007], some laboratory work on such systems exists. Similarly, dissipation in melt-bearing systems has been investigated [*Jackson et al.*, 2004], though incorporating those effects into a global model has proved challenging.

[79] As noted in section 4.1, our long-period results require extrapolation beyond frequencies covered by experiments. Although there is some physical justification for the functional form of our extrapolation, it would clearly be of interest to acquire longer-period dissipation measurements. This is particularly the case given the apparently anomalous frequency-dependence of the lunar Q at tidal periods.

[80] Figure 3 suggests that k_2 and h_2 should exhibit a mild frequency-dependence. Acquisition of high-precision gravity data by the GRAIL spacecraft may test this prediction, and will certainly reduce the current uncertainties in k_2.

[81] Finally, the approach presented here can readily be extended to other bodies. A particularly obvious target is tidal dissipation in Mars, which is hard to understand using Maxwell viscoelasticity [*Bills et al.*, 2005]. The extended Burgers model may very well provide the solution to this particular conundrum.

6. Summary and Conclusions

[82] Our main conclusion is that mantle melting is not required to reproduce the relatively dissipative lunar interior. This is important because recent seismological papers have reached different conclusions on this issue [*Weber et al.*, 2011; *Garcia et al.*, 2011]. It also matters because the presence of a residual mantle melt layer could have significant physical consequences (e.g., sequestration of incompatible, heat-producing elements and water) as well as providing a clue to the earlier state and cooling and volcanic history of the Moon [e.g., *Ziethe et al.*, 2009].

[83] Second, although we cannot constrain total heat production rates directly, our estimate of the present-day mantle heat production rate of 9–10 nWm^{-3} is considerably less than the estimated bulk lunar heat production rates of *Garrick-Bethell et al.* [2010]. This in turn suggests that a significant fraction (≈50%) of heat-producing elements are in the crust and perhaps the shallow upper mantle. Shallow sequestration of radiogenics has implications for the shallow temperature structure and thus issues such as long-term maintenance of topography [e.g., *Lambeck and Pullan*, 1980].

[84] Third, the present-day viscosity at the base of the mantle is sufficiently high that the core-mantle boundary (CMB) would likely be able to maintain a non-equilibrium shape, in agreement with tentative geodetic observations [*Williams et al.*, 2012]. This is important because such a non-equilibrium shape constrains the time-temperature evolution of the lunar interior since the shape was imposed, and thus narrows the range of possible thermal histories.

[85] **Acknowledgments.** We thank Michael Efroimsky and an anonymous reviewer for helpful comments. We are also grateful for discussions with Ian Garrick-Bethell, Philippe Lognonné and Amir Khan. Part of this work was funded by NASA (NNX12AL08G).

References

Aizawa, Y., A. Barnhoorn, U. H. Faul, J. D. F. Gerald, I. Jackson, and I. Kovacs (2008), Seismic properties of anita bay dunite: An exploratory study of the influence of water, *J. Petrol.*, *49*, 841–855.

Bass, J. D. (1995), Elasticity of minerals, glasses and melts, in *Mineral Physics and Crystallography: A Handbook of Physical Constants*, *AGU Ref. Shelf*, vol. 2, edited by T. J. Ahrens, pp. 45–63, AGU, Washington, D. C., doi:10.1029/RF002p0045.

Behounkova, M., G. Tobie, G. Choblet, and O. Cadek (2010), Coupling mantle convection and tidal dissipation: Applications to Enceladus and Earth-like planets, *J. Geophys. Res.*, *115*, E09011, doi:10.1029/2009JE003564.

Bills, B. G., G. A. Neumann, D. E. Smith, and M. T. Zuber (2005), Improved estimate of tidal dissipation within Mars from MOLA observations of the shadow of Phobos, *J. Geophys. Res.*, *110*, E07004, doi:10.1029/2004JE002376.

Blanchette-Guertin, J.-F., C. Johnson, and J. Lawrence (2012), Modeling seismic waveforms in a highly scattering Moon, *Lunar Planet. Sci. Conf.*, *XXXXIII*, Abstract 1473.

Efroimsky, M. (2012), Tidal dissipation compared to seismic dissipation: In small bodies, earths and super-earths, *Astrophys. J.*, *746*, 150.

Efroimsky, M., and J. G. Williams (2009), Tidal torques: A critical review of some techniques, *Celest. Mech. Dyn. Astron.*, *104*, 257–289.

Farla, R. J. M., I. Jackson, J. D. F. FitzGerald, U. H. Faul, and M. E. Zimmerman (2012), Dislocation damping and anisotropic seismic wave attenuation in Earth's upper mantle, *Science*, *336*, 332–335.

Faul, U. H., and I. Jackson (2005), The seismological signature of temperature and grain size variations in the upper mantle, *Earth Planet. Sci. Lett.*, *234*, 119–134.

Faul, U. H., J. D. FitzGerald, and I. Jackson (2004), Shear wave attenuation and dispersion in melt-bearing olivine polycrystals 1. Microstructural interpretation and seismological implications, *J. Geophys. Res.*, *109*, B06202, doi:10.1029/2003JB002407.

Findley, W. N., J. S. Lai, and K. Onaran (1989), *Creep and Relaxation of Nonlinear Viscoelastic Materials*, Dover, Mineola, N. Y.

Gagnepain-Beyneix, J., P. Lognonne, H. Chenet, D. Lombardi, and T. Spohn (2006), A seismic model of the lunar mantle and constraints on temperature and mineralogy, *Phys. Earth Planet. Inter.*, *159*, 140–166.

Gaherty, J. B., and T. H. Jordan (1995), Lehmann discontinuity as the base of an anisotropic layer beneath continents, *Science*, *268*, 1468–1471.

Garcia, R. F., J. Gagnepain-Beyneix, S. Chevrot, and P. Lognonne (2011), Very preliminary reference Moon model, *Phys. Earth Planet. Inter.*, *188*, 96–113.

Garrick-Bethell, I., J. Wisdom, and M. T. Zuber (2006), Evidence for a past high-eccentricity lunar orbit, *Science*, *313*, 652–655.

Garrick-Bethell, I., F. Nimmo, and M. Wieczorek (2010), Structure and formation of the lunar highlands, *Science*, *330*, 949–951.

Goossens, S., et al. (2011), Lunar gravity field determination using selene same-beam differential vlbi tracking data, *J. Geod.*, *85*, 205–228.

Gribb, T. T., and R. F. Cooper (1998), Low-frequency shear attenuation in polycrystalline olivine: Grain boundary diffusion and the physical significance of the andrade model for viscoelastic rheology, *J. Geophys. Res.*, *103*, 27,267–27,279.

Hauri, E. H., T. Weinreich, A. E. Saal, M. C. Rutherford, and J. A. V. Orman (2011), High pre-eruptive water contents preserved in lunar melt inclusions, *Science*, *333*, 213–215.

Hirschmann, M. M. (2000), Mantle solidus: Experimental constraints and the effects of peridotite composition, *Geochem. Geophys. Geosyst.*, *1*(10), 1042, doi:10.1029/2000GC000070.

Hirth, G., and D. Kohlstedt (2003), Rheology of the upper mantle and the mantle wedge: A view from the experimentalists, in *Inside the Subduction Factory*, *Geophys. Monogr. Ser.*, vol. 138, edited by J. Eiler, pp. 83–105, AGU, Washington, D. C., doi:10.1029/138GM06.

Hood, L., F. Herbert, and C. Sonett (1982), The deep lunar electrical conductivity profile: structural and thermal inferences, *J. Geophys. Res.*, *87*, 5311–5326.

Isaak, D. (1992), High-temperature elasticity of iron-bearing olivines, *J. Geophys. Res.*, *97*, 1871–1885.

Jackson, I. (2007), Properties of rocks and minerals: Physical origins of anelasticity and attenuation in rock, *Treatise Geophys.*, *2*, 493–525.

Jackson, I., and U. H. Faul (2010), Grainsize-sensitive viscoelastic relaxation in olivine: Towards a robust laboratory-based model for seismological applications, *Phys. Earth Planet. Inter.*, *183*, 151–164.

Jackson, I., U. Faul, J. FitzGerald, and B. Tan (2004), Shear wave attenuation and dispersion in melt-bearing olivine polycrystals: 1. Specimen fabrication and mechanical testing, *J. Geophys. Res.*, *109*, B06201, doi:10.1029/2003JB002406.

Jolliff, B., J. Gillis, L. Haskin, R. Korotev, and M. Wieczorek (2000), Major lunar crustal terranes: Surface expressions and crust-mantle origins, *J. Geophys. Res.*, *105*, 4197–4216.

Karato, S. (1988), The role of recrystallization in the preferred orientation of olivine, *Phys. Earth Planet. Inter.*, *51*, 107–122.

Karato, S. (2006), Remote sensing of hydrogen in Earth's mantle, *Rev. Mineral. Geochem.*, *62*, 343–375.

Karato, S., and H. Jung (1998), Water, partial melting and the origin of the seismic low velocity and high attenuation zone in the upper mantle, *Earth Planet. Sci. Lett.*, *157*, 193–207.

Karato, S., M. S. Paterson, and J. D. Fitzgerald (1986), Rheology of synthetic olivine aggregates–Influence of grain size and water, *J. Geophys. Res.*, *91*, 8151–8176, 1986.

Khan, A., and K. Moosegaard (2005), Further constraints on the deep lunar interior, *Geophys. Res. Lett.*, *32*, L22203, doi:10.1029/2005GL023985.

Khan, A., K. Mosegaard, J. Williams, and P. Lognonne (2004), Does the Moon possess a molten core? Probing the deep lunar interior results from LLR and Lunar Prospector, *J. Geophys. Res.*, *109*, E09007, doi:10.1029/2004JE002294.

Khan, A., J. Maclennan, S. Taylor, and J. Connelly (2006), Are the Earth and the Moon compositionally alike? Inferences on lunar composition and implications for lunar origin and evolution from geophysical modelling, *J. Geophys. Res.*, *111*, E05005, doi:10.1029/2005JE002608.

Khan, A., J. Connelly, J. Maclennan, and K. Mosegaard (2007), Joint inversion of seismic and gravity data for lunar composition and thermal state, *Geophys. J. Int.*, *168*, 243–258.

Kuskov, O. L., and V. A. Kronrod (2009), Geochemical constraints on the model of the composition and thermal conditions of the Moon according to seismic data, *Phys. Solid Earth*, *45*, 753–768.

Lambeck, K., and S. Pullan (1980), Inferences on the lunar temperature from gravity, stress state and flow laws, *Phys. Earth Planet. Inter.*, *22*, 12–28.

Lee, L. C., S. J. S. Morris, and J. Wilkening (2011), Stress concentrations, diffusionally accommodated grain boundary sliding and the viscoelasticity of polycrystals, *Proc. R. Soc. A*, *467*, 1624–1644.

Lognonne, P. (2005), Planetary seismology, *Ann. Rev. Earth Planet. Sci.*, *33*, 571–604.

Lognonne, P., and C. Johnson (2007), Planetary seismology, *Treatise Geophys.*, *10*, 69–116.

Lognonne, P., and B. Mosser (1993), Planetary seismology, *Surv. Geophys.*, *14*, 239–302.

Minster, J. B., and D. L. Anderson (1981), A model of dislocation-controlled rheology for the mantle, *Philos. Trans. R. Soc. London A*, *299*, 319–356, 1981.

Morris, S. J. S., and I. Jackson (2009), Diffusionally-assisted grain-boundary sliding and viscoelasticity of polycrystals, *J. Mech. Phys. Solids*, *57*, 744–761.

Nakamura, Y. (2005), Farside deep moonquakes and deep interior of the Moon, *J. Geophys. Res.*, *110*, E01001, doi:10.1029/2004JE002332.

Nakamura, Y., and J. Koyama (1982), Seismic Q of the lunar upper mantle, *J. Geophys. Res.*, *87*, 4855–4861.

Nimmo, F., and D. Stevenson (2001), Estimates of Martian crustal thickness from viscous relaxation of topography, *J. Geophys. Res.*, *106*, 5085–5098.

Raj, R., and M. F. Ashby (1971), On grain boundary sliding and diffusional creep, *Metall. Trans.*, *2*, 1113–1127.

Rasmussen, K. L., and P. H. Warren(1985), Megaregolith thickness, heat flow and the bulk composition of the Moon, *Nature*, *313*, 121–124.

Roberts, J. H., and F. Nimmo (2008), Tidal heating and the long-term stability of a subsurface ocean on Enceladus, *Icarus*, *194*, 675–689.

Shito, A., S. Karato, and J. Park (2004), Frequency dependence of Q in Earth's upper mantle inferred from continuous spectra of body waves, *Geophys. Res. Lett.*, *31*, L12603, doi:10.1029/2004GL019582.

Weber, R., P.-Y. Lin, E. Garnero, Q. Williams, and P. Lognonne (2011), Seismic detection of the lunar core, *Science*, *331*, 309–312.

Wieczorek, M., et al. (2006), The constitution and structure of the lunar interior, *Rev. Min. Geochem.*, *60*, 221–364.

Williams, J., D. Boggs, C. Yoder, J. Ratcliff, and J. Dickey (2001), Lunar rotational dissipation in solid body and molten core, *J. Geophys. Res.*, *106*, 27,933–27,968.

Williams, J. G., D. H. Boggs, and J. T. Ratcliff (2012), Lunar moment of inertia, Love number and core, *Lunar Planet. Sci. Conf.*, *XXXXIII*, Abstract 2230.

Zhong, S. J., and M. T. Zuber (2000), Long wavelength topographic relaxation for self-gravitating planets and implications for time-dependent compensation of surface topography, *J. Geophys. Res.*, *105*, 4153–4164.

Zhong, S., C. Qin, G. A, and J. Wahr (2012), Can tidal tomography be used to unravel the long-wavelength structure of the lunar interior?, *Geophys. Res. Lett.*, *39*, L15201, doi:10.1029/2012GL052362.

Ziethe, R., K. Seiferlin, and H. Hiesinger (2009), Duration and extent of lunar volcanism: Comparison of 3D convection models to mare basalt ages, *Planet. Space Sci.*, *57*, 784–796.